A CORRELATION TENSOR–BASED MODEL FOR TIME VARIANT FREQUENCY SELECTIVE MIMO CHANNELS

Martin Weis, Giovanni Del Galdo, and Martin Haardt

Ilmenau University of Technology - Communications Research Laboratory
P.O. Box 100565, 98684 Ilmenau, Germany
martin.weis@stud.tu-ilmenau.de, {giovanni.delgaldo, martin.haardt}@tu-ilmenau.de

ABSTRACT

In this contribution we present a new analytical channel model for frequency selective, time variant MIMO systems. The model is based on a correlation tensor, which allows a natural description of multi–dimensional signals. By applying the Higher Order Singular Value Decomposition (HOSVD), we gain a better insight into the multi–dimensional eigenstructure of the channel. Applications of the model include the denoising of measured channels and the possibility to generate new synthetic channels displaying a given correlation in time, frequency, and space. The proposed model possesses advantages over existing 2–dimensional eigenmode–based channel models. In contrast to them, the tensor–based model can cope with frequency and time selectivity in a natural way.

1. INTRODUCTION

Multiple Input Multiple Output (MIMO) schemes offer the chance to fulfill the challenging requirements for future communication systems, as higher data rates can be achieved by exploiting the spatial dimension. To investigate, design, and test new techniques, it is crucial to use realistic channel models.

We propose a tensor–based analytical channel model which, in contrast to traditional models, can cope with non–stationary time and frequency selective channels. The latter are particularly relevant for wireless communications. We represent the frequency selective, time variant MIMO channel as a 4–dimensional tensor $\boldsymbol{\mathcal{H}} \in \mathbb{C}^{M_\mathrm{R} \times M_\mathrm{T} \times N_\mathrm{f} \times N_\mathrm{t}}$, where M_R and M_T are the number of antennas at the transmitter and receiver, whereas N_f and N_t are the number of samples taken in frequency and time, respectively.

To visualize the spatial structure of the channel, eigenmode–based models have been introduced, such as [1, 2]. However, these models use a 2–dimensional correlation matrix which considers one dimension only. Alternatively, by a cumbersome stacking of the channel coefficients, as in [2], it is possible to consider more dimensions. Moreover, by following this approach, it is not possible to investigate the eigenmodes of different dimensions separately, whereas the proposed tensor–based channel model allows this.

In [3], a tensor–based channel model was introduced. The latter is however a tensor extension of [1], and therefore assumes a Kronecker like structure of the eigenmodes. In this paper, we introduce a more general tensor–based channel model, which truly captures the nature of MIMO channels. The generalized Higher Order Singular Value Decomposition
(HOSVD) [4] gives us the possibility to analyze the eigenstructure of the channel along more dimensions, i.e., along space and frequency.

The paper is organized as follows: Section 2 gives a brief introduction of the relevant tensor algebra, which is needed to understand the proposed model. Section 3 introduces the tensor–based channel model and its applications. Moreover, this section shows the applicability and validity of the model on channel measurements. In Section 4 the conclusions are drawn.

2. BASIC TENSOR CALCULUS

2.1. Notation

To facilitate the distinction between scalars, vectors, matrices and higher–order tensors, we use the following notation: scalars are denoted by lower–case italic letters $(a, b, ...)$, vectors by boldface lower–case italic letters $(\boldsymbol{a}, \boldsymbol{b}, ...)$, matrices by boldface upper–case letters $(\boldsymbol{A}, \boldsymbol{B}, ...)$, and tensors are denoted as upper–case, boldface, calligraphic letters $(\boldsymbol{\mathcal{A}}, \boldsymbol{\mathcal{B}}, ...)$. This notation is consistently used for lower–order parts of a given structure. For example, the entry with row index i and column index j in a matrix $\boldsymbol{A}$ is symbolized by $a_{i,j}$. Furthermore, the i–th column vector of $\boldsymbol{A}$ is denoted as $\boldsymbol{a}_i$. As indices, mainly the letters i, j, k, and n are used. The upper bounds for these indices are given by the upper–case letters I, J, K, and N, unless stated otherwise.

2.2. n–mode vectors and tensor unfoldings

In the (2–dimensional) matrix case we distinguish between row vectors and column vectors. As a generalization of this idea, we build the n–mode vectors $\{\boldsymbol{a}\}$ of an N–th order tensor $\boldsymbol{\mathcal{A}} \in \mathbb{C}^{I_1 \times I_2 \times \cdots \times I_N}$ by varying the index i_n of the elements $\{a_{i_1,...,i_n,...,i_N}\}$ while keeping the other indices fixed. In Figure 1, this is shown for a 3–dimensional tensor. Please note that in general there are $(I_1 \cdot I_2 \cdots I_{n-1} \cdot I_{n+1} \cdots I_N)$ such vectors. In the 2–dimenional case the column vectors are equal to the 1–mode vectors, and the row vectors are equal to the 2–mode vectors. The n–th unfold-

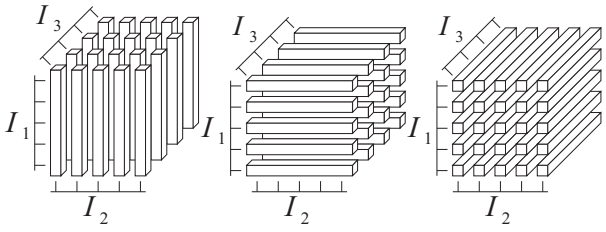

Fig. 1. Mode 1, 2, and 3 vectors of a 3–dimensional tensor.

ing matrix $\boldsymbol{\mathcal{A}}_{(n)} \in \mathbb{C}^{I_n \times (I_1 I_2 \cdots I_{n-1} I_{n+1} \cdots I_N)}$ is the matrix consisting of all n–mode vectors. In [4], the ordering of the n–mode vectors was defined in a cyclic way. In contrast to the definition in [4] we define the n–th unfolding matrix as follows:

$$\boldsymbol{\mathcal{A}}_{[n]} = \{a_{j,k}\} \in \mathbb{C}^{I_n \times (I_1 I_2 \cdots I_{n-1} I_{n+1} I_{n+2} \cdots I_N)} ,$$

with $j = i_n$ and

$$k = 1 + \sum_{l=1, l \neq n}^{N} (i_L - 1) \cdot \prod_{q=1, q \neq n}^{l-1} I_q .$$

This definition assures that the indices of the n–mode vectors vary faster in the following ascending order

$$i_1, i_2, \ldots, i_{n-1}, i_{n+2}, \ldots, i_N . \tag{1}$$

This ordering becomes particularly important for our later derivations, especially for equation (23). Please note that this unfolding definition is also consistent with the MATLAB® command `reshape`. Therefore, we will refer to this unfolding as the MATLAB–like unfolding.

2.3. Tensor operations

2.3.1. The n–mode product

To perform a generalized Higher Order Singular Value Decomposition (HOSVD), it is necessary to transform the n–mode vector space of a tensor. This can be done with the n–mode product between a tensor and a matrix. Let us assume a tensor $\boldsymbol{\mathcal{A}} = \{a_{i_1,i_2,\ldots,i_N}\} \in \mathbb{C}^{I_1 \times I_2 \times \cdots \times I_N}$ and a matrix $\boldsymbol{U} \in \mathbb{C}^{J_n \times I_n}$. Then the n–mode product, denoted by $\boldsymbol{\mathcal{A}} \times_n \boldsymbol{U}$, is a $(I_1 \times I_2 \times \cdots \times I_{n-1} \times J_n \times I_{n+1} \times \cdots \times I_N)$ tensor, whose entries are given by

$$(\boldsymbol{\mathcal{A}} \times_n \boldsymbol{U})_{i_1,i_2,\ldots,i_{n-1},j_n,i_{n+1},\ldots,i_N} = \sum_{i_n=1}^{I_n} a_{i_1,i_2,\ldots,i_{n-1},i_n,i_{n+1}\ldots,i_N} \cdot u_{j_n,i_n} , \tag{2}$$

for all possible values of the indices. With the help of the unfolding definition from above we can write the n–mode product also in terms of matrix operations. Then, the n–th unfolding of the resulting tensor $\boldsymbol{\mathcal{B}}$ can be calculated as

$$\boldsymbol{\mathcal{B}}_{[n]} = \boldsymbol{U} \cdot \boldsymbol{\mathcal{A}}_{[n]} . \tag{3}$$

2.3.2. The outer product

We now define the outer product between 2 tensors. Assume an N–th order tensor $\boldsymbol{\mathcal{A}}$ and a K–th order tensor $\boldsymbol{\mathcal{B}}$. Then, the outer product, denoted as $(\boldsymbol{\mathcal{A}} \circ \boldsymbol{\mathcal{B}})$, is a $(N + K)$–th dimensional tensor whose entries are given by

$$(\boldsymbol{\mathcal{A}} \circ \boldsymbol{\mathcal{B}})_{i_1,i_2,\ldots,i_N,j_1,j_2,\ldots,j_K} = a_{i_1,i_2,\ldots,i_N} \cdot b_{j_1,j_2,\ldots,j_K} ,$$

for all possible values of the indices. Therefore, the outer product creates a tensor with all combinations of possible pairwise element–products.

2.3.3. The n–mode inner product

The n–mode inner product is denoted as $\boldsymbol{\mathcal{A}} = \boldsymbol{\mathcal{B}} \bullet_n \boldsymbol{\mathcal{C}}$. The resulting tensor $\boldsymbol{\mathcal{A}}$ has order $N + K - 2$, where N and K are the orders of $\boldsymbol{\mathcal{B}} \in \mathbb{C}^{I_1 \times \cdots \times I_N}$ and $\boldsymbol{\mathcal{C}} \in \mathbb{C}^{J_1 \times \cdots \times J_N}$, respectively. It is related to the outer product and implies an additional summation over the n–th dimension of both tensors. Therefore, we define the n–mode inner product as

$$\boldsymbol{\mathcal{A}} = \sum_{l=1}^{I_n} \boldsymbol{\mathcal{B}}_{i_n=l} \circ \boldsymbol{\mathcal{C}}_{j_n=l} , \tag{4}$$

where $\boldsymbol{\mathcal{B}}_{i_n=l}$ is the $(N-1)$–th dimensional subtensor of $\boldsymbol{\mathcal{B}}$ which we obtain when we set the index along the dimension n equal to l. The tensor $\boldsymbol{\mathcal{C}}_{j_n=l}$ is defined in an analogous way. Please note that the tensors $\boldsymbol{\mathcal{B}}$ and $\boldsymbol{\mathcal{C}}$ must be of same size along the n–th dimension, and therefore $I_n = J_n$.

2.3.4. The $\mathrm{vec}(\cdot)$ *operator for tensors*

The $\mathrm{vec}(\cdot)$ operator stacks all elements of a tensor into a vector. Thereby the indices i_n of an N–dimensional tensor $\boldsymbol{\mathcal{A}}$ vary in the following ascending order

$$i_1, i_2, \ldots, i_{N-1}, i_N .$$

Please note that the unfolding definition in Section 2.2 ensures that the $\mathrm{vec}(\cdot)$ operation for an N–dimensional tensor is equal to the transpose of its $(N+1)$–th unfolding

$$\mathrm{vec}(\boldsymbol{\mathcal{A}}) = \boldsymbol{\mathcal{A}}_{[N+1]}^{\mathrm{T}} . \tag{5}$$

2.4. Higher Order Singular Value Decomposition

Every N–th order complex tensor $\boldsymbol{\mathcal{A}} \in \mathbb{C}^{I_1 \times I_2 \times \cdots \times I_N}$ can be decomposed into the form

$$\boldsymbol{\mathcal{A}} = \boldsymbol{\mathcal{S}} \times_1 \boldsymbol{U}^{(1)} \times_2 \boldsymbol{U}^{(2)} \cdots \times_N \boldsymbol{U}^{(N)} , \tag{6}$$

in which the matrices of the n–mode singular vectors $\boldsymbol{U}^{(n)} = \left[\boldsymbol{u}_1^{(n)}, \boldsymbol{u}_2^{(n)}, \ldots, \boldsymbol{u}_{I_n}^{(n)}\right] \in \mathbb{C}^{I_n \times I_n}$ are unitary, and the core tensor $\boldsymbol{\mathcal{S}} \in \mathbb{C}^{I_1 \times I_2 \times \cdots \times I_N}$ is a tensor of the same size as $\boldsymbol{\mathcal{A}}$. The basis matrices $\boldsymbol{U}^{(n)}$ contain the left singular vectors $\boldsymbol{u}_1^{(n)}, \boldsymbol{u}_2^{(n)}, \ldots, \boldsymbol{u}_{I_n}^{(n)}$ of the matrix unfoldings $\boldsymbol{A}_{[n]}$. The core tensor $\boldsymbol{\mathcal{S}}$ can be calculated with the equation

$$\boldsymbol{\mathcal{S}} = \boldsymbol{\mathcal{A}} \times_1 \boldsymbol{U}^{(1)^{\mathrm{H}}} \times_2 \boldsymbol{U}^{(2)^{\mathrm{H}}} \cdots \times_N \boldsymbol{U}^{(N)^{\mathrm{H}}} , \tag{7}$$

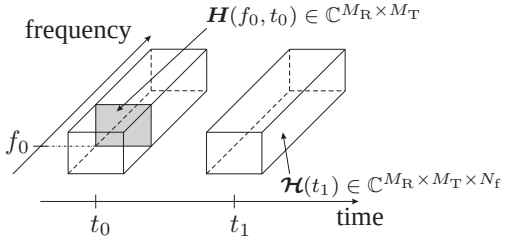

Fig. 2. Definition of the channel tensor. The 2–dimensional subtensor $\boldsymbol{H}(f_0,t_0)$, and the 3–dimensional subtensor $\boldsymbol{\mathcal{H}}(t_1)$ are depicted.

where $(\cdot)^\mathrm{H}$ denotes the Hermitian transpose. The core tensor fulfills some special properties, especially the property of all orthogonality, which means that the rows of all unfolding matrices $\boldsymbol{S}_{[n]}$ are orthogonal, c.f. [4]. With the help of the Kronecker product it is possible to write equation (6) in terms of matrix operations.

$$\boldsymbol{\mathcal{A}}_{[n]} = \boldsymbol{U}^{(n)}\cdot\boldsymbol{\mathcal{S}}_{[n]}\cdot \left(\boldsymbol{U}^{(N)}\otimes\cdots\otimes\boldsymbol{U}^{(n+1)}\otimes\boldsymbol{U}^{(n-1)}\otimes\cdots\otimes\boldsymbol{U}^{(1)}\right)^\mathrm{T}. \quad (8)$$

Please note that this formula is only valid for the MATLAB–like unfolding defined in Section 2.2.

3. TENSOR CHANNEL MODEL

As already mentioned, we represent the channel coefficients in form of the tensor

$$\boldsymbol{\mathcal{H}}\in\mathbb{C}^{M_\mathrm{R}\times M_\mathrm{T}\times N_\mathrm{f}\times N_\mathrm{t}}, \quad (9)$$

where M_R and M_T are the number of antennas at the transmitter and receiver, and N_f and N_t are the number of samples taken in frequency and time, respectively. Please note that the frequency domain of the channel is connected to its delay time τ via a Fourier Transform.

Similarly to [3, 5], we now define the channel correlation tensor as

$$\boldsymbol{\mathcal{R}} = \mathrm{E}\{\boldsymbol{\mathcal{H}}(t)\circ\boldsymbol{\mathcal{H}}(t)^*\}\in\mathbb{C}^{M_\mathrm{R}\times M_\mathrm{T}\times N_\mathrm{f}\times M_\mathrm{R}\times M_\mathrm{T}\times N_\mathrm{f}}, \quad (10)$$

where $\boldsymbol{\mathcal{H}}(t)\in\mathbb{C}^{M_\mathrm{R}\times M_\mathrm{T}\times N_\mathrm{f}}$ is the frequency selective MIMO channel at time snapshot t.

Assuming that the channel is block–wise stationary in time, we define an averaging window of size T_W, so that the channel within the k–th window, denoted with $\boldsymbol{\mathcal{H}}_k$, can be assumed stationary (see Figure 3). The over–all channel matrix $\boldsymbol{\mathcal{H}}$ is then defined as

$$\boldsymbol{\mathcal{H}} = \left[\boldsymbol{\mathcal{H}}_1 \sqcup_4 \boldsymbol{\mathcal{H}}_1 \sqcup_4 \cdots \sqcup_4 \boldsymbol{\mathcal{H}}_{\lfloor\frac{N_t}{T_\mathrm{W}}\rfloor}\right], \quad (11)$$

where $\sqcup_4$ denotes the concatenation of the tensors $\boldsymbol{\mathcal{H}}_k$ along the 4–th dimension, as introduced in [5]. We compute an estimate of the k–th correlation tensor by averaging in time, as

$$\begin{aligned}\boldsymbol{\mathcal{R}}_k \approx \hat{\boldsymbol{\mathcal{R}}}_k &= \frac{1}{T_\mathrm{W}}\cdot\sum_{n=1}^{T_\mathrm{W}}(\boldsymbol{\mathcal{H}}_k)_{i_4=n}\circ(\boldsymbol{\mathcal{H}}_k)^*_{i_4=n}\\ &= \frac{1}{T_\mathrm{W}}\cdot\boldsymbol{\mathcal{H}}_k\bullet_4\boldsymbol{\mathcal{H}}_k^*,\end{aligned} \quad (12)$$

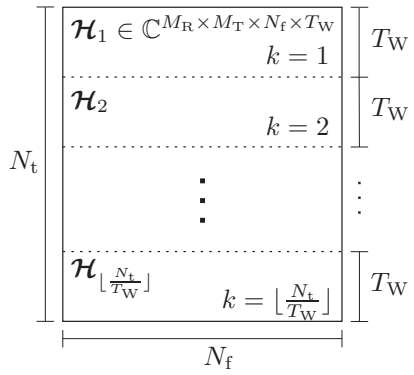

Fig. 3. Definition of the non-overlapping stationarity windows. Each window has T_W time samples. In the other dimensions, each window is of same size as $\boldsymbol{\mathcal{H}}$.

where $\bullet_4$ denotes the 4–mode inner product. Please note that n is the time index within the k–th window. To get insight into the spatial structure of the channel, we decompose this correlation tensor via the following HOSVD

$$\hat{\boldsymbol{\mathcal{R}}}_k = \boldsymbol{\mathcal{S}}_k\times_1\boldsymbol{U}_k^{(1)}\times_2\boldsymbol{U}_k^{(2)}\times_3\boldsymbol{U}_k^{(3)}\times_4\boldsymbol{U}_k^{(4)}\times_5\boldsymbol{U}_k^{(5)}\times_6\boldsymbol{U}_k^{(6)}. \quad (13)$$

The matrices $\boldsymbol{U}_k^{(n)}$ contain the left singular vectors of the n–th unfolding matrices $(\hat{\boldsymbol{R}}_k)_{[n]}$ of $\hat{\boldsymbol{\mathcal{R}}}_k$. The symmetries of the correlation tensor are also reflected by its HOSVD. Therefore, we can choose a HOSVD such that the following equations hold

$$\begin{aligned}\boldsymbol{U}_k^{(1)} &= \boldsymbol{U}_k^{(4)^*},\\ \boldsymbol{U}_k^{(2)} &= \boldsymbol{U}_k^{(5)^*},\\ \boldsymbol{U}_k^{(3)} &= \boldsymbol{U}_k^{(6)^*}.\end{aligned} \quad (14)$$

In this case, equation (13) can be simplified to

$$\begin{aligned}\hat{\boldsymbol{\mathcal{R}}}_k = \boldsymbol{\mathcal{S}}_k &\times_1\boldsymbol{U}_k^{(1)}\times_2\boldsymbol{U}_k^{(2)}\times_3\boldsymbol{U}_k^{(3)}\\ &\times_4\boldsymbol{U}_k^{(1)^*}\times_5\boldsymbol{U}_k^{(2)^*}\times_6\boldsymbol{U}_k^{(3)^*},\end{aligned} \quad (15)$$

and the core tensor $\boldsymbol{\mathcal{S}}_k$, according to Section 2.4, can be calculated via

$$\begin{aligned}\boldsymbol{\mathcal{S}}_k = \hat{\boldsymbol{\mathcal{R}}}_k &\times_1\boldsymbol{U}_k^{(1)^\mathrm{H}}\times_2\boldsymbol{U}_k^{(2)^\mathrm{H}}\times_3\boldsymbol{U}_k^{(3)^\mathrm{H}}\\ &\times_4\boldsymbol{U}_k^{(1)^\mathrm{T}}\times_5\boldsymbol{U}_k^{(2)^\mathrm{T}}\times_6\boldsymbol{U}_k^{(3)^\mathrm{T}}.\end{aligned} \quad (16)$$

The proposed channel model consists in computing the correlation tensors $\hat{\boldsymbol{\mathcal{R}}}_k$ for all windows, i.e., $\forall k=1\ldots\lfloor\frac{N_t}{T_\mathrm{W}}\rfloor$, as they describe exhaustively the correlation properties of the channel, seen as a temporal block stationary stochastic process.

In the following we give a brief description of two applications of the proposed channel model, namely the generation of new channel realizations and the subspace–based denoising of a channel measurement. Then we apply the correlation tensor–based channel model to channel measurements, and compare its performance with the tensor–based channel model presented in [3].

3.1. Channel Synthesis

In the 2–dimensional case [1, 2], the joint spatial correlation matrix is defined as

$$\boldsymbol{R}_k = \mathrm{E}\{\mathrm{vec}(\boldsymbol{\mathcal{H}}_k) \cdot \mathrm{vec}(\boldsymbol{\mathcal{H}}_k)^{\mathrm{H}}\} \,. \tag{17}$$

Similarly to (12), we can compute an estimate of $\boldsymbol{R}_k$, denoted by $\hat{\boldsymbol{R}}_k$ with

$$\hat{\boldsymbol{R}}_k = \frac{1}{T_{\mathrm{W}}} \sum_{n=1}^{T_{\mathrm{W}}} \mathrm{vec}\left((\boldsymbol{\mathcal{H}}_k)_{i_4=n}\right) \cdot \mathrm{vec}\left((\boldsymbol{\mathcal{H}}_k)_{i_4=n}\right)^{\mathrm{H}} \,. \tag{18}$$

From the information given in the correlation matrix $\hat{\boldsymbol{R}}_k$, it is possible to construct a new random synthetic channel $\tilde{\boldsymbol{\mathcal{H}}}_k$, displaying the same spatio–frequency correlation as $\boldsymbol{\mathcal{H}}_k(t)$ via

$$\mathrm{vec}\left(\tilde{\boldsymbol{\mathcal{H}}}_k\right) = \boldsymbol{X}_k \cdot \boldsymbol{g} \,, \tag{19}$$

where the entries of the vector $\boldsymbol{g}$ are i.i.d. zero mean complex Gaussian random numbers with unit variance, and

$$\boldsymbol{X}_k = \hat{\boldsymbol{R}}_k^{\frac{1}{2}} \,. \tag{20}$$

The matrix $\boldsymbol{X}_k$ is computed via a 2–dimensional eigenvalue decomposition of

$$\hat{\boldsymbol{R}}_k = \boldsymbol{U}_k \cdot \boldsymbol{\Sigma}_k \cdot \boldsymbol{U}_k^{\mathrm{H}} \,, \tag{21}$$

where the matrix $\boldsymbol{U}_k$ contains all eigenvectors of $\hat{\boldsymbol{R}}_k$ and $\boldsymbol{\Sigma}_k$ is the diagonal matrix containing the eigenvalues. Then we define $\boldsymbol{X}_k$ as follows

$$\hat{\boldsymbol{R}}_k^{\frac{1}{2}} = \boldsymbol{U} \cdot \boldsymbol{\Sigma}^{\frac{1}{2}} = \boldsymbol{X}_k \,. \tag{22}$$

By computing the matrix $\boldsymbol{X}_k$ we can generate new random synthetic channels by means of equation (19). In the following we show that it is also possible to compute the matrix $\boldsymbol{X}_k$ from the HOSVD of the correlation tensor $\hat{\boldsymbol{\mathcal{R}}}_k$.

With the help of the MATLAB–like unfolding from Section 2, the connection between the estimated 2D correlation matrix $\hat{\boldsymbol{R}}_k$ and the estimated correlation tensor $\hat{\boldsymbol{\mathcal{R}}}_k$ is given by

$$\mathrm{vec}\left(\hat{\boldsymbol{R}}_k\right) = \left(\hat{\boldsymbol{R}}_k\right)_{[3]}^{\mathrm{T}} = \left(\hat{\boldsymbol{\mathcal{R}}}_k\right)_{[7]}^{\mathrm{T}} = \mathrm{vec}\left(\hat{\boldsymbol{\mathcal{R}}}_k\right) \,. \tag{23}$$

To compute the matrix $\boldsymbol{X}_k$, we can either compute a SVD of $\hat{\boldsymbol{R}}_k$, or apply a HOSVD on $\hat{\boldsymbol{\mathcal{R}}}_k$. This relation between the 2–dimensional model and the correlation tensor–based model follows from the following derivation. For the reason of simplicity we first define the following unitary matrix:

$$\boldsymbol{U}_k^{\mathrm{e}} = \boldsymbol{U}_k^{(3)} \otimes \boldsymbol{U}_k^{(2)} \otimes \boldsymbol{U}_k^{(1)} \,. \tag{24}$$

With the Kronecker version of the HOSVD (8) it follows from the latter relation

$$\begin{aligned} \mathrm{vec}\left(\hat{\boldsymbol{R}}_k\right) = \mathrm{vec}\left(\hat{\boldsymbol{\mathcal{R}}}_k\right) &= \left(\hat{\boldsymbol{\mathcal{R}}}_k\right)_{[7]}^{\mathrm{T}} \\ &= \left(\boldsymbol{U}_k^{\mathrm{e}^*} \otimes \boldsymbol{U}_k^{\mathrm{e}}\right) \cdot (\boldsymbol{\mathcal{S}}_k)_{[7]}^{\mathrm{T}} \\ &= \mathrm{vec}\left(\boldsymbol{U}_k^{\mathrm{e}} \cdot \mathrm{unvec}_{I\times I}\left((\boldsymbol{\mathcal{S}}_k)_{[7]}^{\mathrm{T}}\right) \cdot \boldsymbol{U}_k^{\mathrm{e}^{\mathrm{H}}}\right) \,. \end{aligned}$$

Here $\mathrm{unvec}_{I\times I}\left((\boldsymbol{\mathcal{S}}_k)_{[7]}^{\mathrm{T}}\right)$ denotes the inverse matrix $\mathrm{vec}(\cdot)$ operation applied to the 7–th unfolding of the core tensor $\boldsymbol{\mathcal{S}}_k$. Therefore, $\mathrm{unvec}_{I\times I}\left((\boldsymbol{\mathcal{S}}_k)_{[7]}^{\mathrm{T}}\right)$ is a square matrix of same size as $\hat{\boldsymbol{R}}_k$ with $I = M_{\mathrm{R}} M_{\mathrm{T}} N_f$. The correlation matrix $\hat{\boldsymbol{R}}_k$ can be calculated from the HOSVD of the tensor $\hat{\boldsymbol{\mathcal{R}}}_k$ via

$$\hat{\boldsymbol{R}}_k = \boldsymbol{U}_k^{\mathrm{e}} \cdot \mathrm{unvec}_{I\times I}\left((\boldsymbol{\mathcal{S}}_k)_{[7]}^{\mathrm{T}}\right) \cdot \boldsymbol{U}_k^{\mathrm{e}^{\mathrm{H}}} \tag{25}$$

Please note that $\mathrm{unvec}_{I\times I}\left((\boldsymbol{\mathcal{S}}_k)_{[7]}^{\mathrm{T}}\right)$ is not a diagonal matrix. Therefore, we have to perform an additional SVD for the calculation of $\boldsymbol{X}_k$, as follows

$$\mathrm{unvec}_{I\times I}\left((\boldsymbol{\mathcal{S}}_k)_{[7]}^{\mathrm{T}}\right) = \boldsymbol{V}_k \cdot \tilde{\boldsymbol{\Sigma}}_k \cdot \boldsymbol{V}_k^{\mathrm{H}} \,.$$

Now the matrix $\boldsymbol{X}_k$ can be calculated as

$$\boldsymbol{X}_k = \left(\boldsymbol{U}_k^{(3)} \otimes \boldsymbol{U}_k^{(2)} \otimes \boldsymbol{U}_k^{(1)}\right) \cdot \boldsymbol{V}_k \cdot \tilde{\boldsymbol{\Sigma}}_k^{\frac{1}{2}} \,. \tag{26}$$

Especially in cases, where $\tilde{\boldsymbol{\Sigma}}_k$ is of low rank it is computationally cheaper to calculate $\boldsymbol{X}_k$ directly from $\hat{\boldsymbol{\mathcal{R}}}_k$ using equation (26).

3.2. Denoising a Measured Channel

In order to reduce the noise in measured channels, we extend an idea proposed in [2] to the correlation tensor–based channel model. For every window k, as defined above, we construct a tensor $\boldsymbol{\mathcal{Z}}_k(t)$, calculated for every time snapshot t, using the following equation

$$\boldsymbol{\mathcal{Z}}_k(t) = \boldsymbol{\mathcal{H}}_k(t) \times_1 \boldsymbol{U}_k^{(1)^{\mathrm{H}}} \times_2 \boldsymbol{U}_k^{(2)^{\mathrm{H}}} \times_3 \boldsymbol{U}_k^{(3)^{\mathrm{H}}} \,, \tag{27}$$

where the matrices $\boldsymbol{U}_k^{(n)}$ are computed from the correlation tensor $\hat{\boldsymbol{\mathcal{R}}}_k$ given in (12). With the help of the tensor $\boldsymbol{\mathcal{Z}}_k(t)$, the channel can be reconstructed exactly via the synthesis equation

$$\boldsymbol{\mathcal{H}}_k(t) = \boldsymbol{\mathcal{Z}}_k(t) \times_1 \boldsymbol{U}_k^{(1)} \times_2 \boldsymbol{U}_k^{(2)} \times_3 \boldsymbol{U}_k^{(3)} \,. \tag{28}$$

Denoising the measurement tensor $\boldsymbol{\mathcal{H}}_k(t)$ is possible by simply considering only the first L_n singular vectors of $\boldsymbol{U}_k^{(n)}$, corresponding to the L_n largest singular values of $\hat{\boldsymbol{R}}_k$. L_n should be determined with the help of the singular value spectra of the HOSVD. This is similar to the well known low–rank approximation of a matrix via the 2D SVD. Thereby, we assume that the omitted singular vectors span the noise space. Thus, we obtain the tensor $\boldsymbol{\mathcal{Z}}'_k(t) \in \mathbb{C}^{L_1\times L_2\times L_3}$ and

$$\begin{aligned} (\boldsymbol{\mathcal{H}}_k)_{\mathrm{denoised}}(t) = &\boldsymbol{\mathcal{Z}}'_k(t) \times_1 \left(\boldsymbol{U}_k^{(1)}\right)^{[L_1]} \\ &\times_2 \left(\boldsymbol{U}_k^{(2)}\right)^{[L_2]} \times_3 \left(\boldsymbol{U}_k^{(3)}\right)^{[L_3]} \,, \end{aligned} \tag{29}$$

where $\left(\boldsymbol{U}_k^{(n)}\right)^{[L_n]}$ indicates the matrix containing the first L_n singular vectors along the n-th dimension and for the k-th window.

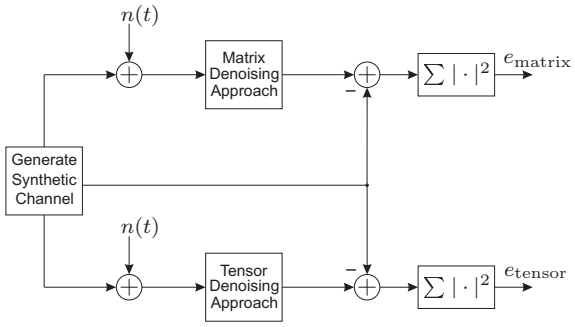

Fig. 4. Block diagramm of the performance test for the 2 denoising approaches.

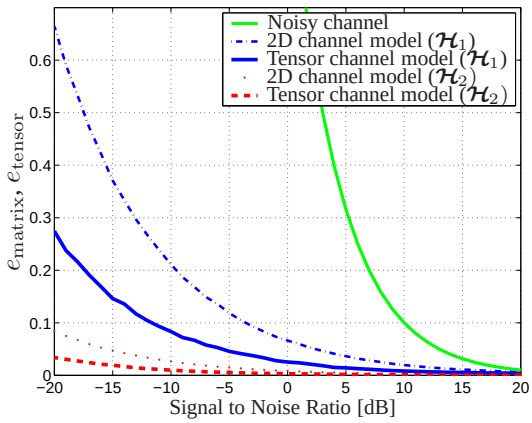

Fig. 5. Reconstruction error for two synthetic noisy channels: a rich multi–path channel $\boldsymbol{\mathcal{H}}_1$; a 2–path channel $\boldsymbol{\mathcal{H}}_2$. The tensor–based denoising outperforms the 2D approach for richer channels. The green curve represents the error for the noisy channels.

Figure 5 shows the reconstruction error for two noisy synthetic channels, namely $\boldsymbol{\mathcal{H}}_1$ and $\boldsymbol{\mathcal{H}}_2$, and two denoising approaches. The channels are created with the IlmProp, a flexible geometry based channel model capable of generating frequency selective time variant multi–user MIMO channels displaying realistic correlation in frequency, time, space, and between users, cf. [6]. The Figures 7 and 6 show the geometries of the synthetic channels. The first channel $\boldsymbol{\mathcal{H}}_1$, is richer in multi-path components than the second $\boldsymbol{\mathcal{H}}_2$. The reconstruction error (power) is defined as the Euclidian distance between the noiseless channel and the reconstructed (denoised) channel

$$e_x = \sum_{n=1}^{N_{\text{f}} M_{\text{R}} M_{\text{T}}} \left| \text{vec}\left(\boldsymbol{\mathcal{H}}_{\text{synthetic}}\right)_n - \text{vec}\left(\boldsymbol{\mathcal{H}}_{\text{denoised}}\right)_n \right|^2 , \tag{30}$$

for $x = \{\text{matrix}, \text{tensor}\}$, as also depicted Figure 4. In Figure 5, the thick lines represent the error obtained via the proposed tensor–based method. The thin lines show the reconstruction error achieved by applying a low–rank approximation directly on $\hat{\boldsymbol{R}}$. We can observe that the tensor–based approach leads to a better subspace estimate, because of the additional singular vectors in the frequency direction. This translates to a lower reconstruction error. The gain with respect to the 2D approach becomes more relevant for richer channels.

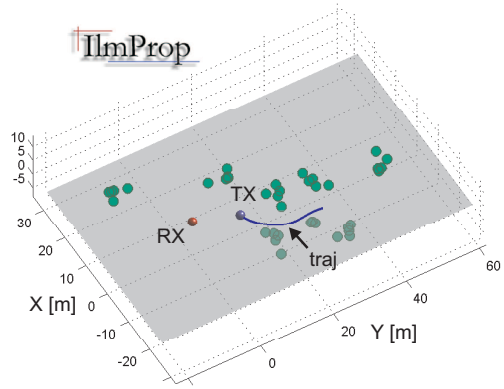

Fig. 6. Synthetic IlmProp scenario characterized by rich scattering ($\boldsymbol{\mathcal{H}}_1$)

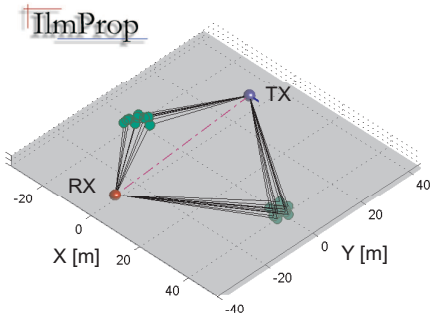

Fig. 7. Synthetic IlmProp scenario characterized by 2 paths ($\boldsymbol{\mathcal{H}}_2$)

3.3. Validation on Measurements

Next, we apply the proposed correlation tensor–based model on measurements gathered from the main train station in Munich, Germany. The multi-dimensional RUSK MIMO channel sounder employed a 16×8 antenna architecture with a 16–element uniform circular array (UCA) at the transmitter and an 8–element uniform linear array (ULA) at the receiver. The antenna spacing at both arrays was about $\lambda/2$. The bandwidth was 120 MHz at a carrier frequency of 5.2 GHz. The frequency spacing was 3.125 kHz which yields a total of 385 frequency bins. The receiver measured a complete channel response every 18.432 ms. A total of 9104 time snapshots were taken. The mobile terminal was moving in a Non Line-Of-Sight (NLOS) regime. The environment was particularly rich in multi-path components.

For the calculation of the channel model we consider only 25 adjacent frequency bins around the center frequency, thus spanning a bandwidth of 7.5 MHz. We divide the channel into windows of $T_{\text{W}} = 25$ samples in the time domain, as in Figure 3.

We first consider 10 adjacent time windows of the measured channel. To assess the behavior of the channel in the frequency domain, we compare the proposed correla-

tion tensor–based channel model with the model presented in [3] by means of the ergodic capacity

$$C = \mathrm{E}\left\{\log_2\left[\det\left(\boldsymbol{I}_{M_\mathrm{R}} + \frac{\rho}{M_\mathrm{T}}\boldsymbol{H}_{f,t}\cdot\boldsymbol{H}_{f,t}^\mathrm{H}\right)\right]\right\}.$$

Numerically, the equation above is computed for subbands of 5 frequency samples each and by averaging in time and frequency in every window, so that

$$C = \frac{1}{F}\frac{1}{T_\mathrm{W}}\sum_{f,t}\log_2\left[\det\left(\boldsymbol{I}_{M_\mathrm{R}} + \frac{\rho}{M_\mathrm{T}}\boldsymbol{H}_{f,t}\cdot\boldsymbol{H}_{f,t}^\mathrm{H}\right)\right],$$

where $F = 5$, and $T_\mathrm{W} = 25$. For the observed 10 windows, we obtain a total of $5 \cdot 10 = 50$ capacity estimates.

From each window, using all 25 frequency bins, we compute the correlation tensor as in equation (12) and the parameters for the model proposed in [3], which we refer to as the *structured model*. Please note that we do not compare our model with existing 2–dimensional ones (such as Kronecker [7] or Weichselberger [1]), because they are not suitable for modeling the channel in the frequency dimension. With the tensor–based models we generate new channel tensors with exactly the same sizes as the measured one. We then compute the capacities in the way just mentioned and we plot the results in Figure 8

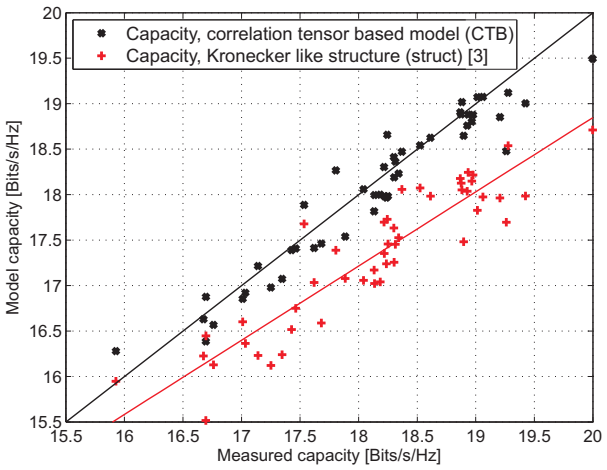

Fig. 8. Capacity comparison between the proposed model and the structured model [3]. The closer the points are to the diagonal, the more precisely the modeled capacity fits the capacity of the channel.

We can see that the proposed correlation tensor–based model performs better than the *structured model*. Since the estimate of the ergodic capacity is computed from very few samples, its variance is presumably large. To avoid this problem and eliminate any influence of the estimation errors on the performance of the two models, we follow the processing scheme depicted in Figure 9. From one measurement window we compute a reference correlation tensor $\hat{\boldsymbol{\mathcal{R}}}_\mathrm{ref}$ and from it, using equation (19), we generate 30000 new channel realizations. The latter are used to compute the capacity C_MEAS which we take as reference. From the new realizations we calculate the parameters for both models and compare the modeled capacities to C_MEAS. The capacity of the proposed model is denoted by C_CTB, as for Correlation Tensor–Based (CTB), whereas the structured model from [3] is denoted by C_struct. The results are given in Figure 10. Theoretically, the reference capacity C_MEAS and the capacity obtained from the proposed model C_struct must be equal, as they are calculated with the same channel model. As we take a finite number of samples, the two capacities still differ slightly, i.e., the C_struct are not on the diagonal. Also in this case, the proposed channel model shows a better performance than the *structured model*.

From the results shown in Figures 8 and 10, we can see that the proposed method achieves a higher accuracy, although the gap in capacity to the structured model is not large. As these figures refer to particular time snapshots of a specific channel measurement, we now investigate how the performances change with different propagation conditions. To do so, we divide once more the measurement tensor $\boldsymbol{\mathcal{H}}$ into windows of 25 time and frequency samples. Then, for each window, we compute the distance between the correlation tensors $\boldsymbol{\mathcal{R}}_\mathrm{CTB}$ (correlation tensor–based model) and $\boldsymbol{\mathcal{R}}_\mathrm{struct}$ (*structured model*), by means of a straightforward extension of the metric proposed in [8]. It is defined as

$$D = 1 - \frac{\langle \mathrm{vec}\left(\boldsymbol{\mathcal{R}}_\mathrm{CTB}\right), \mathrm{vec}\left(\boldsymbol{\mathcal{R}}_\mathrm{struct}\right)\rangle}{\|\mathrm{vec}\left(\boldsymbol{\mathcal{R}}_\mathrm{CTB}\right)\|_\mathrm{F}\cdot\|\mathrm{vec}\left(\boldsymbol{\mathcal{R}}_\mathrm{struct}\right)\|_\mathrm{F}}, \qquad (31)$$

where $\langle\cdot,\cdot\rangle$ denotes the scalar product, and $\|\cdot\|_\mathrm{F}$ is the Frobenius norm. The latter ranges in the interval $[0,\ 1]$, and becomes larger, the more the signal spaces of the two correlation tensors overlap. The metric becomes zero for non–overlapping, orthogonal signal subspaces. Figure 11 depicts the results of this comparison (top plot) and the power of the channel (bottom one). Simulations show that for lower values of the metric, the structured model performs worse, as it is incapable of mimicking the full statistics of the channel. We can observe that there is a correlation between the power of the channel and the metric D, and thus, between the power and the performance of the model proposed in [3]. This can be interpreted as follows. For smaller powers, the channel is richer in multi-path, and the eigenstructure of the correlation tensor can be better represented by a Kronecker–like structure.

The validity of this observation needs to be investigated further with the help of additional channel measurements. In particular, the capacity might not be the best metric to compare these models, as it is computed independently for each frequency bin, and therefore, does not account for any correlation along this dimension.

The portion of the channel used for the capacity comparison from the Figures 8 and 10 are highlighted in Figure 11. In the time windows for which the metric D is high, both models show the same performance with respect to the capacity.

4. CONCLUSIONS

We present a novel correlation tensor–based channel model which is applicable for frequency selective, time vari-

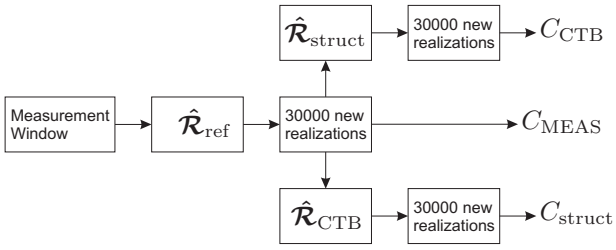

Fig. 9. Capacity comparison out of the reference tensor, taken from the above measurements.

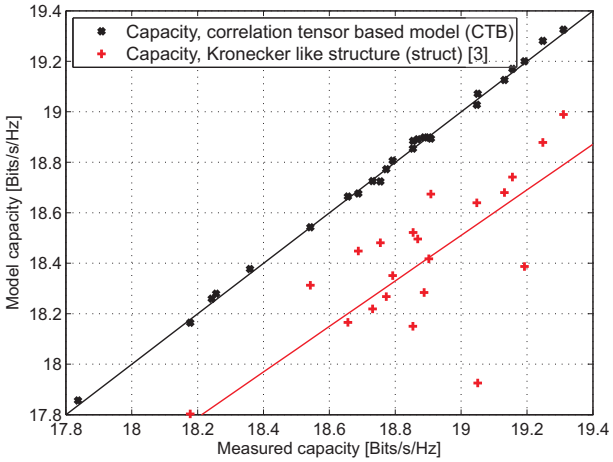

Fig. 10. Results of the capacity comparison

ant MIMO channels. We assume temporal block-wise stationarity. The tensor calculus allows us to analyze the channel eigenmodes also along the frequency dimension, permitting us to cope with frequency selective channels as well. The model lets us generate new random channels which display given correlation properties in space and frequency. Moreover, the tensor–based approach yields an efficient denoising application for channel measurements, due to an improved subspace estimate. Moreover, the applicability and validity of the proposed model is proven on channel measurements.

ACKNOWLEDGEMENTS

A part of this work has been performed in the framework of the IST project IST-4-027756 WINNER II, which is funded by the European Union. The authors also gratefully acknowledge the support of the German Research Foundation (Deutsche Forschungsgemeinschaft, DFG) under contract no. HA 2239/1-2.

The authors also would like thank Prof. Thomä (Electronic Measurement Research Lab, TU Ilmenau) for providing the measurement data. Those have been performed in the framework of the WIGWAM project, funded by German Federal Ministry of Research and Education (BMBF).

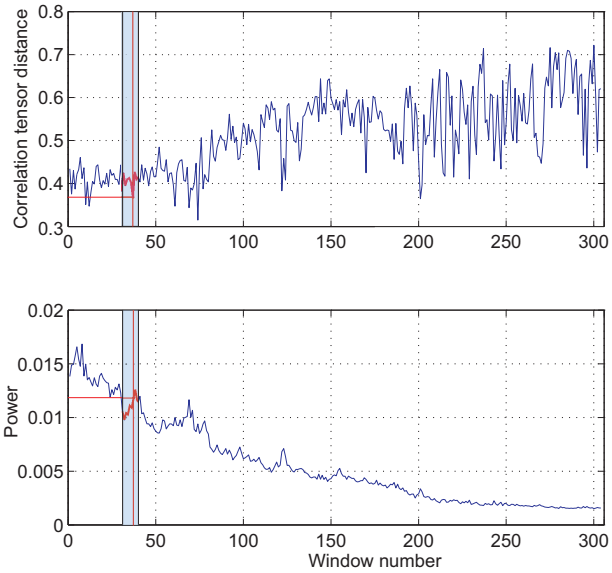

Fig. 11. Distance of the correlation tensors (after Herdin) for the Kronecker like model after [3] and the correlation tensor–based model. The lower part of the picture draws the power profile of the channel.

REFERENCES

[1] W. Weichselberger, M. Herdin, H. Özcelik, and E. Bonek, "A stochastic MIMO channel model with joint correlation of both link ends," *IEEE Trans. on Wireless Comm.*, vol. 5, no. 1, pp. 90–100, Jan. 2006.

[2] G. Del Galdo, M. Haardt, and M. Milojevic, "A subspace-based channel model for frequency selective time variant MIMO channels," in *Proc. 15th Int. Symp. on Personal, Indoor, and Mobile Radio Communications (PIMRC)*, Barcelona, Spain, Sept. 2004.

[3] N. Costa and S. Haykin, "A novel wideband MIMO channel model and McMaster's wideband MIMO SDR," *Asilomar Conf. on Signals, Systems, and Computers*, Nov. 2006., to be published.

[4] L. de Lathauwer, B. de Moor, and J. Vandewalle, "A multilinear singular value decomposition," *SIAM J. Matrix Anal. Appl.*, vol. 21, no. 4, 2000.

[5] F. Römer, M. Haardt, and G. Del Galdo, "Higher order SVD based subspace estimation to improve multi-dimensional parameter estimation algorithms," in *40th Asilomar Conf. on Signals, Systems, and Computers*, Pacific Grove, CA, US, Nov. 2006.

[6] G. Del Galdo, M. Haardt, and C. Schneider, "Geometry-based channel modelling of MIMO channels in comparison with channel sounder measurements," *Advances in Radio Science - Kleinheubacher Berichte*, pp. 117–126, October 2003, more information on the model, as well as the source code and some exemplary scenarios can be found at http://tu-ilmenau.de/ilmprop.

[7] C.-N. Chuah, J. M. Kahn, and D. Tse, "Capacity of multi-antenna array systems in indoor wireless environment," *IEEE Global Telecommunications Conference, Sydney, Australia, 1998*, vol. 5, pp. 1894–1899, 1998.

[8] M. Herdin, "Non – stationary indoor MIMO radio channels," *Ph.D. Dissertation, Technische Universität Wien, Austria*, 2004.